www.czasopisma.pan.pl PAN POLSKA AKADEMIA NAUK www.journals.pan.pl

Arch. Min. Sci. **65** (2020), 1, 129-146

Electronic version (in color) of this paper is available: http://mining.archives.pl

DOI 10.24425/ams.2020.132711

YANAN SUN[1,2], PEISEN ZHANG[1,2*], WEI YAN[1,2],
FENQIAN YAN[1,2], JUNDA WU[1,2]

COMPRESSIVE DEFORMATION CHARACTERISTICS OF CRUSHED SANDSTONE BASED ON MULTIPLE EXPERIMENTAL FACTORS

In this study, the compressive deformation of crushed sandstone was tested using a crushed rock deformation-seepage test system, and the effects of various factors, including crushed rock grade, grade combination, water saturation status, and stress loading method (i.e., continuous loading or cyclic loading and unloading), on the compressive deformation of crushed sandstone was analyzed from four perspectives including stress-strain, bulking coefficient, deformation mechanism and energy dissipation. The results indicate that the stress-strain relations of crushed sandstone are closely associated with all factors considered, and are well represented by exponential functions. The strain observed for a given applied stress increased with increasing crushed rock grade throughout the loading period. Crushed sandstone grades were combined according to a grading index (n), where the proportion of large-grade rocks in the sample increased with increasing n. The bearing capacity of a water-saturated crushed sandstone sample with $n = 0.2$ was less than that of an equivalent dry sample for a given applied stress. The stress-strain curve of a water-saturated crushed sandstone sample with $n = 0.2$ under cyclic loading and unloading was similar to that obtained under continuous loading. Observation and discovery, the deformation mechanism of crushed sandstone was mainly divided into four stages, including crushing, rupture, corner detachment and corner wear. And 20% of the work done by testing machine is used for friction between the crushed sandstone with the inner wall of the test chamber, and 80% is used for the closing of the void between the crushed sandstone, friction sliding, crushing damage.

Keywords: rock mechanics, saturated graded crushed rock, compressive deformation, cyclic loading and unloading

[1] SHANDONG UNIVERSITY OF SCIENCE AND TECHNOLOGY, STATE KEY LABORATORY OF MINING DISASTER PREVENTION AND CONTROL, QINGDAO 266590, CHINA
[2] MINING ENGINEERING NATIONAL EXPERIMENTAL TEACHING DEMONSTRATION CENTER, QINGDAO 266590, CHINA

* Correspondin author: sky_0826@163.com

© 2020. The Author(s). This is an open-access article distributed under the terms of the Creative Commons Attribution-NonCommercial License (CC BY-NC 4.0, https://creativecommons.org/licenses/by-nc/4.0/deed.en which permits the use, redistribution of the material in any medium or format, transforming and building upon the material, provided that the article is properly cited, the use is noncommercial, and no modifications or adaptations are made.

1. Introduction

In the longwall mining of coal seems, the roof is systematically collapsed as the seam is mined out, and the loosely packed collapsed material within the mined-out area functions as support for the overlying strata. Consequently, the mechanical properties of crushed rock materials from the roof of a mined-out coal seam have always been an important focus of geotechnical engineering and mining engineering because these materials are highly vulnerable to large compressive deformation owing to the repeated action of groundwater and the weight of the overlying strata, which can lead to overlying strata collapse and ground surface subsidence. Therefore, investigating the compressive deformation characteristics of crushed rock materials in mined-out areas is essential for evaluating the potential for overlying strata collapse and the extent of ground surface subsidence.

In recent years, many scholars have conducted a large number of experimental studies focused on the bulking and compaction characteristics of crushed rock materials. For example, Liao et al. (1997).conducted a systematic study on the compaction characteristics of rock and coal, and measured their bulking coefficients, bulking curves, compaction curves, and lateral compression curves. Later, a large number of scholars conducted compaction tests for crushed rock materials with different lithologies, such as coal, shale, sandstone, sandy mudstone, and mudstone, and evaluated the stress-strain relationship during compaction (Lee et al., 2018; Wang et al., 2014). while the size of crushed rock in the collapse zone varies substantially, and the rock grade distribution can be regarded as continuous(Feng et al., 2016). This dimensionality feature of crushed rock is particularly challenging for conducting tests under realistic experimental conditions. The influence of the Talbol power index on the compressive deformation and fractal characteristics of rock samples has also been examined (Yu et al., 2014, 2016; Arasan et al., 2011; Lima et al., 2016; Wang et al., 2014). In addition, researchers have analyzed the influences of various factors, such as different Loading method, loading rate, and axial compression displacement, on the compressive deformation and fractal characteristics of rock samples (Cieslik et al., 2013; Kwasniewski et al., 2013; Singh et al., 2016). Moreover, different water immersion times have been demonstrated to greatly affect the physical and mechanical parameters of crushed rock (Baud et al., 2000; Chen et al., 2018; Xiong et al., 2011; Li et al., 2018; Liu et al.,). Crushed coal and rock subjected to cyclic loading and unloading tests have exhibited obvious cyclic hysteresis loops (Badge & Petros, 2005; Fan et al., 2016; Deng et al., 2017; Liu et al., 2011, 2016; Zhu et al., 2019). The energy dissipation characteristics were also analyzed by calculating the strain energy density. (Deng et al., 2016; Peng et al., 2014; Xiao et al., 2010; Yu et al., 2018; Zhou et al., 2016) .Further, acoustic emission technology provides important information for further understanding the fracture and destruction modes of rock (Cao et al., 2015; Fortin et al., 2009; Liang et al., 2017; Liu et al., 2018; Meng et al., 2018; Xia et al., 2014). Because the environment in which crushed rock is located in actual projects is dangerous and concealed, the development of numerical simulation models that can reflect the fracture characteristics of coal and rock in actual formations can be an extremely effective method for ensuring the safety of underground engineering activities (Ju et al., 2018; Abdia et al., 2017; Duan et al., 2017; Liu et al., 2017).

As indicated above, past studies have demonstrated that the mechanical properties of crushed rock materials observed under the effects of cyclic loading of overlying strata and the extent of saturation by groundwater are important factors influencing the long-term stability of mining

engineering projects. However, most current studies have considered the effect of only a single factor on the deformation characteristics of crushed rock, such as stress-strain curve analysis during rock compaction, loading and unloading responses under a water saturation condition, and energy dissipation at different temperature levels, whereas few studies have considered multifactor cases, which can be expected to provide more accurate models of the compressive deformation characteristics of crushed rock materials in underground mining operations. Note that most coal mining operations are deployed within sedimentary rock, which is primarily sandstone. Apart from factors, such as its mineral composition, structure, and cementation type, the load of overlying strata and groundwater saturation are also vital factors influencing the mechanical properties of sandstone. Therefore, studying the compressive deformation characteristics of water-saturated crushed sandstone under cyclic loading and unloading is of significant value for evaluating ground surface subsidence and surrounding rock deformation in mined-out areas. Finally, it must be noted that, because the deformation, strength characteristics, and mechanical characteristics of fracture damage of crushed rock materials are closely associated with the stress state and the history of stress loading, rocks are vulnerable to fatigue and deformation under cyclic stress loading and unloading. Therefore, studying the stress states of crushed rock materials and stress loading methods reveal important information regarding the compressive deformation mechanisms of water-abundant strata in practical engineering operations. In light of these issues, the present work conducts compressive deformation testing of crushed sandstone that considers crushed rock grade, grade combination, water saturation status, and stress loading condition (i.e., continuous and cyclic loading and unloading) to determine the compressive deformation characteristics of rock materials. All four factors are analyzed quantitatively and comparatively from the perspective of the stress-strain features observed during compaction. The present study also addresses the challenges associated with the dimensionality feature of crushed rock by adopting Talbol continuous grading theory (Zha et al., 2009) to describe the grade distribution of crushed rock. This study provides important practical and theoretical guidance for evaluating ground surface subsidence and surrounding rock deformation in mined-out areas.

2. Materials and methods

2.1. Materials

In this study, foliated sandstone extracted deep from a coal mine of the Anhui Hengyuan Coal Industry and Electricity Power Co. was selected and processed into standard samples using the determination method for characterizing the physical-mechanical properties of rock. The basic physical-mechanical parameters of these samples were tested, and the results are listed in Table 1.

TABLE 1

Standard physical parameters of foliated sandstone

Density (ρ; g·cm^{-3})	Compression strength (σ_c; MPa)	Tensile strength (σ_t; MPa)	Elastic modulus (E_T; GPa)	Poisson's ratio (ν)	Cohesion stress (c; MPa)	Internal friction angle (φ; °)
2.52	45.11	5.71	25.1	0.25	28.2	32.6

The foliated sandstone was crushed mechanically, and, to comply with standard engineering practice, the range of crushed rock grades was set to 0-10 cm based on a field investigation of multiple mined-out areas. The crushed sandstone was screened into five groups with crushed rock grades of 0-2 cm, 2-4 cm, 4-6 cm, 6-8 cm, and 8-10 cm, as shown in Figure 1.

Fig. 1. Distribution of crushed sandstone grades

1) Five groups crushed sandstone based on rock grade

To ensure that a consistent volume of crushed sandstone was employed for each grade during testing, each test sample was placed in the test chamber at a natural packing height (h) of about 32 cm. Here, the stacking height can only be close to 32 cm due to the different sizes and characteristics of the crushed sandstone grains. However, the error in the values of h between the different test samples was less than 0.5 cm. The packing parameters of the test samples for each rock grade are listed in Table 2.

TABLE 2

Crushed sandstone packing parameters according to rock grade

Grade ID	Grade (cm)	Height (m)	Weight (kg)	Volume (m^3)	Packing density (kg/m^3)
Grade 1	0-2	0.3228	56.44	0.04054619	1392
Grade 2	2-4	0.3211	51.25	0.04032388	1271
Grade 3	4-6	0.3207	47.78	0.04028243	1186
Grade 4	6-8	0.3226	46.39	0.04051354	1145
Grade 5	8-10	0.3191	45.57	0.04007519	1137

Here, the packing density (kg/m^3) of crushed sandstone in the test chamber is calculated as the ratio of the sample mass m to sample volume V in the test chamber as follows:

$$\rho = \frac{m}{V} = \frac{m}{A \cdot h} \tag{1}$$

where A is the cross-sectional area of the test chamber (m^2).

2) Seven groups crushed sandstone based on grading index *n*

Because the crushed rock materials in a caving zone vary largely in size, their grade distribution can be considered continuous. Therefore, the present study also considered different combinations of crushed sandstone grades assembled from the five grades according to Talbol continuous grading theory. Here, the grading index n of crushed sandstone is calculated as follows:

$$\frac{M_d}{M_t} = \left(\frac{d}{D}\right)^n \times 100\% \tag{2}$$

where d is the grade of crushed rock (cm), D is the maximum grade of crushed rock (cm), M_d is the weight of crushed rock less than or equal to d, M_t is the total weight of crushed rock.

The percentages the different crushed rock grades by weight employed to obtain the seven grading indexes (n) adopted in the present work are listed Table 3.

TABLE 3

Percentages of crushed sandstone grades by weight for each Talbol index (i.e., grading index n)

Talbol Index (n)	Percentage of crushed sandstone grades by weight				
	0-2 cm (wt%)	2-4 cm (wt%)	4-6 cm (wt%)	6-8 cm (wt%)	8-10 cm (wt%)
0.2	72.48	10.78	7.04	5.34	4.36
0.3	61.70	14.26	9.82	7.74	6.48
0.4	52.54	16.78	12.2	9.94	8.54
0.5	44.72	18.52	14.22	11.98	10.56
0.6	38.08	19.64	15.90	13.86	12.52
0.7	32.42	20.04	17.28	15.60	14.46
0.8	27.60	20.46	18.40	17.20	16.34

2.2. Test System

The crushed rock deformation-seepage test system is used for compaction testing in this study. The principal structure and parameters of this system are shown in Figure 2. The system consists

Fig. 2. Structure and system parameters of the crushed rock deformation-seepage test system

of loading head, test chamber, water pressure chamber, energy storage tank, work station, water pressure-volume double-control servo system, and displacement-stress double-control servo system. Briefly, a uniform volume of crushed sandstone was placed in the test chamber, and subjected to compression under controlled water saturation conditions by the loading head under control of the displacement-stress double-control servo system, and the stress-strain data was recorded. The main parameters of the crushed rock deformation-seepage test system are listed Table 4.

TABLE 4

Main parameters of the crushed rock deformation-seepage test system

	Maximum	**Accuracy**
Shaft pressure	600 KN	0.01 KN
Water pressure	4 MPa	0.01 MPa
Flow	150 L/h	0.15 L/h
Loading head stroke	400 mm	0.01 mm
Test chamber height	380 mm	0.01 mm
Test chamber diameter	400 mm	0.01 mm

2.3. Test Scheme

Four different tests were conducted with the test conditions listed in Table 5 to investigate the effects of rock grade, grading index, water saturation status, and loading method on the stress-strain, bulking coefficient, deformation mechanism of crushed sandstone during compaction. It is important to point out that NWCL (no water, continuous loading), NWCL(n) (grading index was n, no water, continuous loading), FSCL (full saturated, continuous loading), FSLU (full saturated, loading and unloading). Stress grades and duration setting for each stages listed in Table 6.

TABLE 5

Test conditions employed for all compressive deformation

	Grade (cm)	**Grading index (n)**	**Saturation state**	**Loading rate**	**Loading range**	**Loading method**
NWCL	0-2	—	No water	0.5 kN/s	0-450 kN	Continuous loading
	2-4	—				
	4-6	—				
	6-8	—				
	8-10	—				
NWCL(n)	—	0.2	No water	0.5 kN/s	0-450 kN	
	—	0.3				
	—	0.4				
	—	0.5				
	—	0.6				
	—	0.7				
	—	0.8				
FSCL	—	0.2	Full saturation	0.5 kN/s	0-450 kN	
FSLU	—	0.2	Full saturation	0.5 kN/s	0-450 kN	Cyclic loading and unloading

TABLE 6

Stress grades and duration setting for each stage

Grade ID	1	2	3	4	5	6	7	8	9
Shaft pressure (KN)	50	100	150	200	250	300	350	400	450
Stress (MPa)	0.39	0.79	1.19	1.59	1.99	2.39	2.79	3.18	3.57
Duration (min)	30	50	70	90	110	130	150	170	190

Here, the full saturation condition was attained by Vacuum saturation device, filling all the voids between the individual grains with water. The continuous loading method applied an axial stress of 0 to 450 kN to the samples at a constant rate of 0.5 kN/s. The cyclic loading and unloading process involved eight loading stages conducted at a constant rate of 0.5 kN/s. For example, the first stage beginning at 50 kN, when loading to 100 KN and keeping 50min followed by immediate unloading to 50 kN. The maximum applied axial stress of the individual loading stages began at 50 kN and increased in increments of 50 kN at each stage up to 450 kN at stage 8.

According to standard engineering practice, the nominal axial stress of a crushed rock sample is defined as

$$\sigma = \frac{P}{A} \tag{3}$$

where P is the axial load applied to the crushed rock sample (N). The nominal axial strain of a crushed rock sample is defined as

$$\varepsilon = \frac{\Delta h}{h} \tag{4}$$

where Δh is the change in the packing height of the sample in the test chamber, or the amount of compression (cm). The Void fraction of crushed rock is defined as

$$p = \frac{A(h-\Delta h) - \dfrac{m}{\rho_0}}{A(h-\Delta h)} = 1 - \frac{m}{A(h-\Delta h)\rho_0} \tag{5}$$

where ρ_0 is the density of Sandstone (g/cm) (using the determination method for density, $\rho_0 = 2.524$ g/cm).

The bulking coefficient is usually used to represent the characteristics that the volume of rock decreases gradually after compaction and finally reaches a stable value. The bulking coefficient is defined as

$$K = \frac{V_1}{V_0} = \frac{(h-\Delta h)A}{hA} = 1 - \frac{\Delta h}{h} \tag{6}$$

where V_1 is the volume after compressive deformation (cm^3), V_0 is the initial volume of crushed sandstone (cm^3).

3. Results and analysis

3.1. Compressive Deformation of Crushed Sandstone of Various Factors

1) Compressive Deformation of Crushed Sandstone with Different Grades

Samples of the five crushed sandstone grades were subjected to the compaction deformation procedure outlined as NWCL in Table 5, and the stress-strain curves are shown in Figure 3. As shown in the figure, all five grades of the crushed sandstone samples provided an essentially equivalent stress-strain behavior representative of a progressively increasing increment in stress with a corresponding decreasing increment in stain. Here, an equivalent applied axial stress resulted in a greater strain for the 8-10 cm grade than for the 0-2 cm grade, indicating that the relatively large grades are more vulnerable to deformation under loading than the small grades, and therefore compacted more readily.

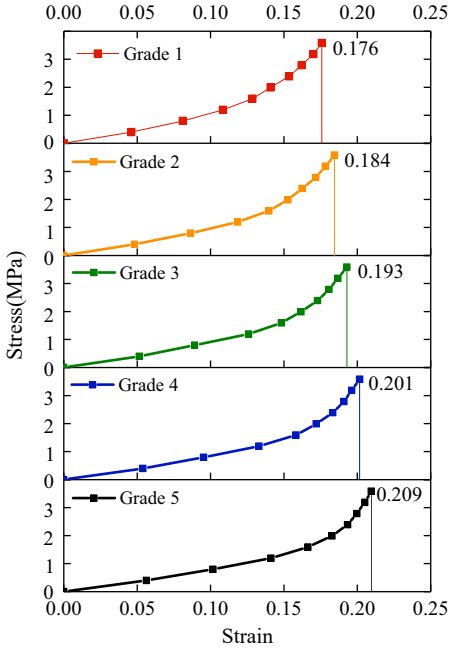

Fig. 3. Stress-strain curves for NWCL

Conducted linear regression analysis of the stress-strain curves obtained for the five crushed sandstone grades based on the following expression:

$$\sigma = \alpha e^{\beta\varepsilon} \tag{7}$$

where α and β are regression coefficients related to the lithological characteristics of the crushed sandstone grades. Here, taking the natural logarithm of both sides yields the linear equation

$\ln(\sigma) = \ln(\alpha) + \beta\varepsilon$. The results of fitting to this linear function based on the experimentally obtained values of σ and ε are listed in Table 7. From the table, Note that the squared correlation coefficients (R^2) obtained for the fitting results were all greater than 0.98. Therefore, the stress-strain curves of the crushed sandstone grades were uniformly represented by Equation (7).

TABLE 7

Stress-strain relations of the different grades of crushed sandstone

Grade ID	Grade (cm)	Regression equation	Square of correlation coefficient (R^2)
Grade 1	0-2	$\sigma = 0.0411e^{24.634\varepsilon}$	$R^2 = 0.9873$
Grade 2	2-4	$\sigma = 0.0484e^{23.288\varepsilon}$	$R^2 = 0.9861$
Grade 3	4-6	$\sigma = 0.0784e^{19.874\varepsilon}$	$R^2 = 0.9959$
Grade 4	6-8	$\sigma = 0.0983e^{18.216\varepsilon}$	$R^2 = 0.9983$
Grade 5	8-10	$\sigma = 0.1253e^{16.366\varepsilon}$	$R^2 = 0.9972$

The linear regression results of the present work for crushed sandstone of different grades is compared with the linear regression results obtained by past studies for crushed coal and shale with equivalent grades in Table 8. In addition, the compression strengths and the ranges of α and β are compared for the three rock materials. Note from the table that the values of α and β for the different crushed rock materials of equivalent grades exhibited uniform tendencies. Here, the values of α and β are observed to increase with increasing compression strength for the different rock materials, and that α and β also increase with increasing grade for the same rock material. As such, the deformation characteristics of the crushed rock materials under pressure

TABLE 8

Uniaxial compression strength of rock material

Rock type	Reference	Uniaxial compression strength	Grade	Regression equation	Range of regression coefficient α	Range of regression coefficient β
Coal	[Chu et al., 2017]	15 MPa	Grade 1	$\sigma = 0.0221e^{5.7602\varepsilon}$	0.0221-0.0870	5.7602-7.2273
			Grade 2	$\sigma = 0.0517e^{6.2147\varepsilon}$		
			Grade 3	$\sigma = 0.1046e^{7.0153\varepsilon}$		
			Grade 4	$\sigma = 0.0726e^{6.5928\varepsilon}$		
			Grade 5	$\sigma = 0.0870e^{7.2273\varepsilon}$		
Shale	[Ma et al., 2005]	25 MPa	Grade 1	$\sigma = 0.0414e^{8.1461\varepsilon}$	0.0414-0.1925	8.1461-10.332
			Grade 2	$\sigma = 0.0717e^{8.2814\varepsilon}$		
			Grade 3	$\sigma = 0.1521e^{9.2727\varepsilon}$		
			Grade 4	$\sigma = 0.166e^{10.2541\varepsilon}$		
			Grade 5	$\sigma = 0.1925e^{10.332\varepsilon}$		
Sandstone	This paper	45 MPa	Grade 1	$\sigma = 0.0411e^{24.634\varepsilon}$	0.0411-0.1253	16.366-24.634
			Grade 2	$\sigma = 0.0484e^{23.288\varepsilon}$		
			Grade 3	$\sigma = 0.0784e^{19.874\varepsilon}$		
			Grade 4	$\sigma = 0.0983e^{18.216\varepsilon}$		
			Grade 5	$\sigma = 0.1253e^{16.366\varepsilon}$		

are reflected by the variations in α and β to some extent. Therefore, referring to the regression coefficients in the stress-strain regression equations reflecting the lithological characteristics and grade distributions of crushed rock materials could provide early prediction for controlling overlying rock deformation in practical longwall mining operations. In particular, the ranges of these coefficients are of substantial reference value for this purpose.

2) Compressive Deformation of Crushed Sandstone with Different Grading Indexes

Samples of the crushed sandstone grades in the seven different grading indexes were subjected to the compaction deformation procedure outlined as NWCL(n) in Table 5, and the strain -time curves are shown in Figure 4. It can be seen from the figure that the strain of all groups of graded sandstone combinations increased more rapidly than the applied axial stress in the early period of loading. However, the increase in strain became increasingly less apparent when the applied axial stress exceeded 1.2 MPa, while the differences between the strains of the various groups at the same applied axial stress increased. Note that the strain of the groups obtained at the same applied axial stress increased with increasing n.

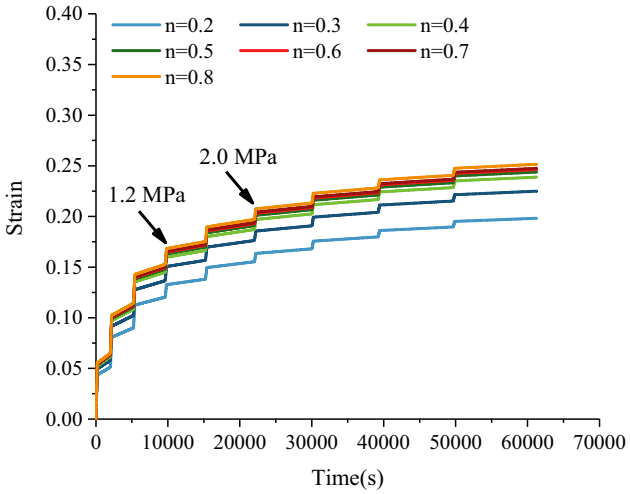

Fig. 4. Stress-time curves for NWCL(n)

The observed compaction behavior in the initial stress loading period (0-1.2 MPa) here was primarily caused by the many readily compressible voids of different sizes between the individual grains of the samples. In the middle stress loading period (1.2-2.0 MPa), the preliminarily compacted individual grains have formed a stable structure with greater resistance to further deformation, and the stress begins to increase more rapidly than the strain. The significant differences developing between the strains of the various groups at the same applied axial stress can be attributed to the percentage of large-grade grains in the various groups. Here, the ratio of empty space to filled space (i.e., the void ratio) increased with increasing n, making groups with larger void ratios more vulnerable to deformation, such that the strain of groups at the same applied axial stress increased with increasing n.

3) Compressive Deformation of Saturated Crushed Sandstone (n = 0.2)

A fully saturated crushed sandstone sample with n = 0.2 was subjected to the compaction deformation procedure outlined as FSCL in Table 5, and the strain -time curve for this condition is compared with that obtained for an equivalent sample under the dry condition in Figure 4. It can be seen from figure 5 that the strain of the water-softened sample is significantly greater than that of the dry sample for a given applied axial stress. This is because the cohesion between rock grains in the sample is weakened due to water softening. In addition, the strength of inter-granular connections between the individual particles within the rock grains decreased as water molecules permeated the grains. Thus, the energy required for grain fracture decreased, making the samples more vulnerable to deformation under loading.

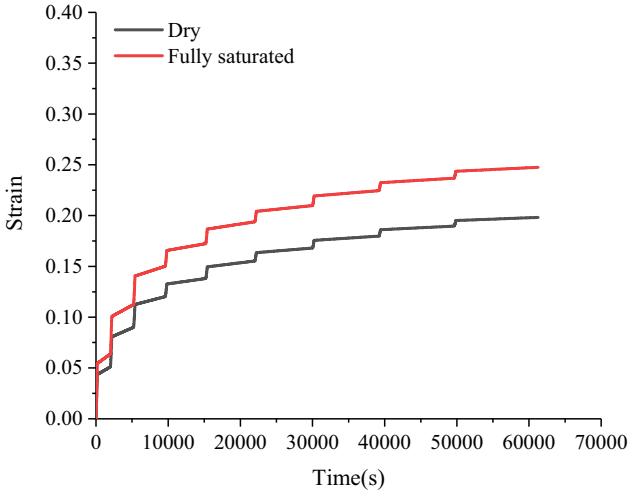

Fig. 5. Stress-time curves of FSCL

4) Compressive Deformation of Saturated Crushed Sandstone (n = 0.2) Under Cyclic Loading and Unloading

A fully saturated crushed sandstone sample with n = 0.2 was subjected to the cyclic loading and unloading compaction deformation procedure outlined as FSLU in Table 5, and the results for this condition are shown in Figure 6(a). It can be seen from Figure 6(a) that the stress-strain behavior of the saturated sample was again exponential under cyclic loading and unloading.

It can be seen from Figure 6(a) with Figure 6(b) that the values of Strain difference gradually decreased from an initial value of 0.03729 to 0.00958 with an increasing number of cycles of unloading. This can be attributed to the progressive destruction of the skeletal structure of the different crushed rock samples as the number of loading and unloading cycles increased. Here, the crushed stones of each crushed rock grade are mutually compacted at the beginning of cyclic loading and unloading to form a relatively stable overall resistance to external loads. In addition, it can be seen from Figure 6(a) that the values of strain is slightly restored in the initial unloading stage, the crushed stone is in the elastic deformation range at this stage.

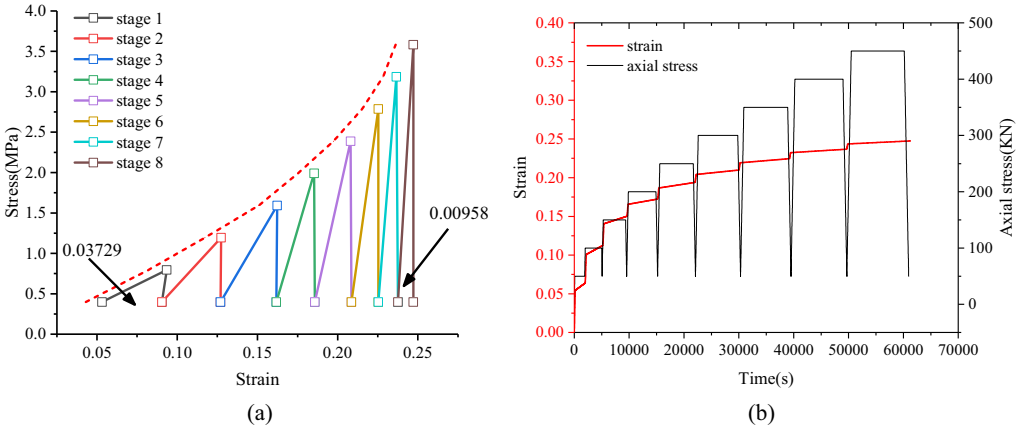

Fig. 6. Stress-strain (a) and strain – time (b) characteristics of FSLU

Figure 7 compares the strain-time curve obtained with a fully saturated crushed sandstone sample (n = 0.2) subjected to cyclic loading and unloading with that obtained for an equivalent sample subjected to continuous loading (i.e., FSCL in Table 4). Note from the strain-time curves that the strain increased more rapidly under continuous loading in the initial period than under cyclic loading and unloading, but that the strain obtained under cyclic loading and unloading increased more rapidly than under continuous loading in the later period.

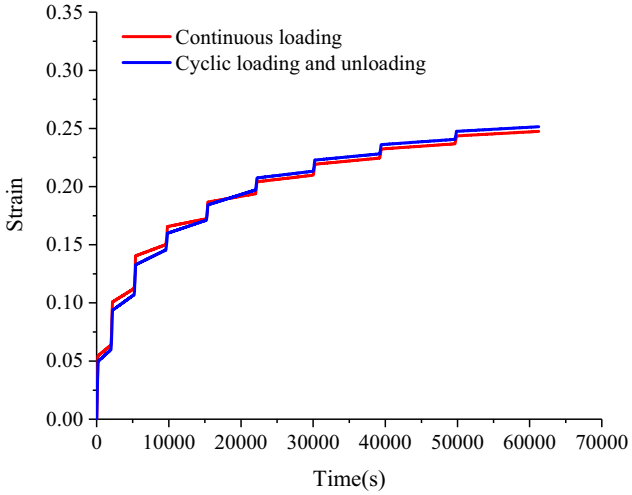

Fig. 7. Strain-time curves of FSCL with FSLU

5) Comparisons of the Four Test Results

The results of the four tests discussed above demonstrate that, under an equivalent stress, the strain of water-saturated samples was greater than that of dry samples, while the strain of samples

under cyclic loading and unloading was greater than that obtained under continuous loading. A comparison of the maximum strain of samples with $n = 0.2$ obtained at the terminal applied stress of 450 kN is also of interest. Here, note that a maximum strain of 0.215 was obtained for the dry sample under continuous loading (NWCL(n)). In contrast, the maximum strains of the water-saturated sample under continuous loading (test 3) and under cyclic loading and unloading (FSLU) were greater than that obtained for NWCL(n) by factors of 1.15 and 1.25, respectively. Thus, the results demonstrate that water saturation and cyclic loading and unloading degraded the pressure-bearing capacity of the crushed sandstone samples to different degrees.

3.2. Bulking Coefficient of Crushed Sandstone

The bulking coefficient of crushed sandstone was tested using a crushed sandstone deformation-seepage test system, the displacement data changes was recorded by the loading head. Void fraction and bulking coefficient of crushed sandstone were calculated by Equation (5) with (6). The results are shown in Figure 8. (Limited to the length of the article, only the results of $n = 0.2$ are listed here.)

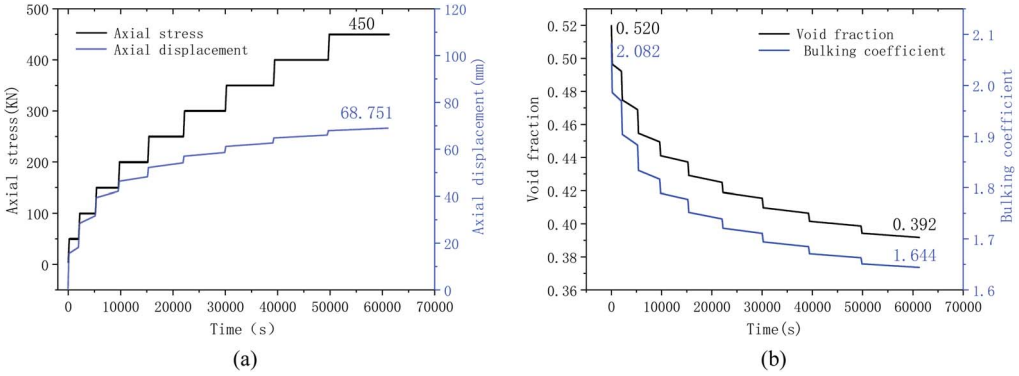

Fig. 8. Compressive deformation of crushed sandstone under the dry condition ($n = 0.2$)

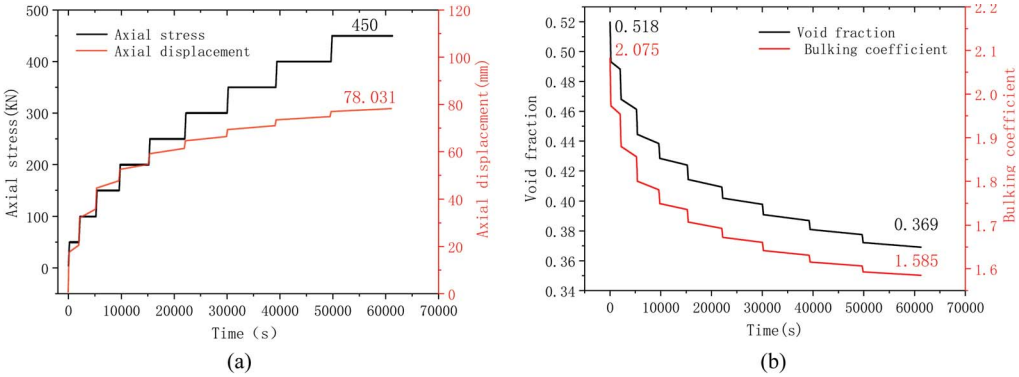

Fig. 9. Compressive deformation of saturated crushed sandstone ($n = 0.2$)

It can be seen from Figure 8(a) that the values of axial displacement gradually increased from an initial value of 0.01 to 68.751 with an increasing number of continuous loading. However, for each loading stage, the axial displacement increased more rapidly under continuous loading period than under constant loading. The increase of axial displacement for each loading stage was decreased gradually with an increasing number of Continuous loading.

The values of void fraction of crushed sandstone was gradually decreased from an initial value of 0.520 to 0.392 and bulking coefficient was decreased from 2.082 to 1.644 with an increasing number of Continuous loading, as shown in Figure 8(b). As for saturated crushed sandstone, the changes of axial displacement, void fraction, bulking coefficient were similar to that crushed sandstone under the dry condition, as shown in Figure 9(a) and Figure 9(b).

3.3. Deformation Mechanism of Crushed Sandstone

Through the observation of the crushed sandstone during the test, the deformation mechanism of crushed sandstone is mainly divided into four stages, as shown in Figure 10.

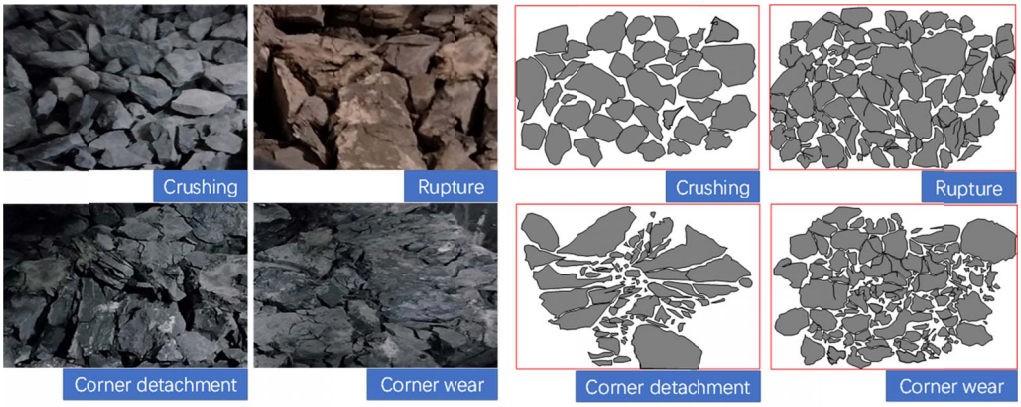

Fig. 10. Four stages of crushed sandstone deformation mechanism

These results reflect the standard processes of crushed sandstone compaction, which include crushing, rupture, corner detachment, and corner wear. In the initial continuous stress loading period, the individual grains of the sandstone samples primarily constitute point-to-point contacts with good connectivity in a loose framework containing large voids. However, with increasing applied axial stress, the overall capacity of the rock samples for resisting deformation declined while the degree of deformation developed rapidly, resulting in relative displacement between rock grains and the progressive fracture of individual grains that filled voids via grain rearrangement and with the smaller fragments, and thus rapidly making a more compact structure. The processes of crushing, rupture, corner detachment, and wear progressively transformed the form of grain contact from point-to-point into point-to-surface and surface-to-surface, resulting in rapidly decreasing rock deformation due to an increased capacity for the samples to resist deformation. This analysis also clarifies why the compaction process was increasingly rapid in the order from the 0-2 cm grade to the 8-10 cm grade.

4. Conclusion

The present work conducted compressive deformation testing of crushed sandstone from the effects of various factors, including crushed rock grade, grade combination, water saturation status, and stress loading method (i.e., continuous loading or cyclic loading and unloading), on the compressive deformation of crushed sandstone was analyzed from four perspectives including stress-strain, bulking coefficient, deformation mechanism and energy dissipation. The results provided the following conclusions.

1) In the loading process, the strain of the larger crushed rock grades increases rapidly, and the stress-strain relationships of the individual grade samples can be well represented by exponential functions, and crushed sandstone grades were combined according to a grading index (n), where the proportion of large-grade rocks in the sample increased with increasing n.
2) Due to the effect of water softening, the bearing capacity of the water-saturated crushed sandstone sample with $n = 0.2$ was less than that of the dry sample for a given applied stress. And the stress-strain curve of the water-saturated crushed sandstone sample with $n = 0.2$ under cyclic loading and unloading was similar to that obtained under continuous loading, where both presented an exponential relationship.
3) The work done by the testing machine is mainly consumed by the compaction deformation of the crushed sandstone and the friction between the crushed sandstone with the inner wall of the test chamber. And 20% of the work done by testing machine is used for friction between the crushed sandstone with the inner wall of the test chamber, and 80% is used for the closing of the void between the crushed sandstone , friction sliding, crushing damage.

The present study focused on compressive deformation characteristics obtained under relatively low applied axial stress. Therefore, future studies could include the entire process from initial loading to maximum loading. In addition, improving the visibility of the crushed stone materials within the test chamber would provide additional information regarding the migration and rearrangement of rock materials in the initial loading period and their compressive deformation characteristics at various stages of loading. Finally, the use circulating water flow in the test chamber would simulate the effect of water in a mined-out area more accurately by providing realistic conditions of water erosion that affect the migration of small-grade rocks in the sample.

Data Availability

The data used to support the findings of this study are available from the corresponding author upon request.

Conflicts of Interest

The authors declare that there is no conflict of interest regarding the publication of this paper.

Funding Statement

The authors acknowledge the financial support from the National Key R&D Program of China (2018YFC0604702), the National Natural Science Foundation of China (51509149, 51379119, 51774199), Shandong Key Research and Development Plan (2018GSF120009), the Key Technology Project for Safe Production and Heavy Accident Prevention and Control (gaoxiao-0008-2017AQ, shandong-0016-2018AQ), Special Project of First-class Discipline for Mining Engineering Construction (01CK00605, 03CK01702).

Acknowledgments

Thank you for the conditions provided by Professor Zhang and the help provided by our research team.

References

Arasan S., Akbulut S., Hasiloglu A.S., 2011. *The Relationship Between the Fractal Dimension and Shape Properties of Particles.* KSCE Journal of Civil Engineering **15** (7), 1219-1225.

Abdia M., Molladavoodi H., Salarirad H., 2017. *Rock Failure Analysis Based on A Coupled Elastoplastic-logarithmic Damage Model*. Archives of Mining Sciences **62** (4), 753-774.

Baud P., Zhu W., Wong T.F., 2000. *Failure Mode and Weakening Effect of Water On Sandstone*. Journal of Geophysical Research Solid Earth **105** (B7), 16371-16389.

Bagde M. N., Petroš V., 2005. *The Effect of Machine Behaviour and Mechanical Properties of Intact Sandstone Under Static and Dynamic Uniaxial Cyclic Loading*. Rock Mechanics and Rock Engineering **38** (1), 59-67.

Chu T.X., Li P., Zhao J.K., Yu M. G., Han X.F., 2017. *Bulking Coefficient Evolution Characteristics and Mechanism of Compacted Broken Coal*. Journal of China Coal Society **42** (12), 3182-3188.

Chen Y.L., Yu B.Y., Zhang K., Zhang M.W., Xu G., Chen Z.Q., 2018. *Permeability Evolution and Particle Size Distribution of Saturated Crushed Sandstone Under Compression*. Geofluids, 2018, 1-12.

Cao A.Y., Jing G.C., Dou L.M., Wang G.F., Liu S., Wang C.B., Yao X.X., 2015. *Damage Evolution Law Based on Acoustic Emission of Sandy Mudstone Under Different Uniaxial Loading Rate*. Journal of Mining & Safety Engineering **32** (6), 923-925,935.

Cieslik J., Godyn K., 2013. *Microscopic Analysis of Shear Bands Formation in Luna Limestone Under Quasistatic Triaxial Loading Conditions*. Archives of Mining Sciences **58** (2), 317-332.

Deng H.F., Hu Y., Li J.L., Wang Z., Zhang X.J., Hu A.L., 2016. *The Evolution of Sandstone Energy Dissipation Under Cyclic Loading and Unloading*. Chinese Journal of Rock Mechanics and Engineering **35** (S1), 2869-2875.

Deng H.F., Hu Y., Li J.L., Wang Z., Zhang X.J., Zhang H.B., 2017. *Effects of Frequency and Amplitude of Cyclic Loading On the Dynamic Characteristics of Sandstone*. Rock and Soil Mechanics **38** (12), 3402-3409.

Duan K., Kwok C.Y., Ma X., 2017. *Dem Simulations of Sandstone Under True Triaxial Compressive Tests*. Acta Geotechnica **12** (3), 495-510.

Fan J.Y., Chen J., Jiang D.Y., Ren S., Wu J.X., 2016. *Fatigue Properties of Rock Salt Subjected to Interval Cyclic Pressure.* International Journal of Fatigue **90** (9), 109-115.

Feng M.M., Wu J.Y., Chen Z.Q., Mao X.B., Yu B.Y., 2016. *Experimental Study On the Compaction of Saturated Broken Rock of Continuous Gradation*. Journal of China Coal Society **41** (9), 2195-2202.

Fortin J., Stanchits S., Dresen G., Gueguen Y., 2009. *Acoustic Emissions Monitoring During Inelastic Deformation of Porous Sandstone: Comparison of Three Modes of Deformation*. Pure and Applied Geophysics **166** (5-7), 823-841.

Ju Y., Sun H.F., Xing M.X., Wang X.F., Zheng J.T., 2018. *Numerical Analysis of the Failure Process of Soil–rock Mixtures through Computed Tomography and PFC3D Models*. International Journal of Coal Science & Technology **5** (2), 126-141.

Kwasniewski M., 2013. *Recent Advances in Studies of the Strength of Rocks Under Ture Triaxial Compression Conditions*. Archives of Mining Sciences **58** (4), 1177-1200.

Liao X.X., Mao X.B., Hu G.W., Ma Z.G. 1997. *Research on Broken Expand and Characteristics of Rocks and Coals*. Journal of Experimental Mechanics **12** (3), 64-70.

Lee K., Song C.G., Kim D., 2018. *Evaluation of Compaction and Crushing Characteristics of Frozen and Unfrozen Sands Under Repetitive Compactions*. KSCE Journal of Civil Engineering **22** (9), 3321-3330.

Liu Y., Dai F., Zhao T., Xu N.W., 2017. *Numerical Investigation of the Dynamic Properties of Intermittent Jointed Rock Models Subjected to Cyclic Uniaxial Compression*. Rock Mechanics & Rock Engineering **50**, 89-112.

Liu Y., Dai F., Dong L., Xu N.W., Feng P., 2018. *Experimental Investigation on the Fatigue Mechanical Properties of Intermittently Jointed Rock Models Under Cyclic Uniaxial Compression with Different Loading Parameters*. Rock Mechanics & Rock Engineering **51** (1), 47-68.

Liu E.L., He S.M., Xue X.H., Xu J., 2011. *Dynamic Properties of Intact Rock Samples Subjected to Cyclic Loading Under Confining Pressure Conditions*. Rock Mechanics & Rock Engineering **44** (5), 629-634.

Liang Y.P., Li Q.M., Gu Y.L., Zou Q.L., 2017. *Mechanical and Acoustic Emission Characteristics of Rock: Effect of Loading and Unloading Confining Pressure At the Postpeak Stage*. Journal of Natural Gas Science and Engineering **44**, 54-64.

Liu B., Ma Y.J., Zhang G., Xu W., 2018. *Acoustic Emission Investigation of Hydraulic and Mechanical Characteristics of Muddy Sandstone Experienced One Freeze-thaw Cycle*. Cold Regions Science & Technology **151**, 335-344.

Li Y., Zhang S., Zhang X., 2018. *Classification and Fractal Characteristics of Coal Rock Fragments Under Uniaxial Cyclic Loading Conditions (Article)*. Arabian Journal of Geosciences **11** (9).

Lima C., Motta L., 2016. *Study of Permanent Deformation and Granulometric Distribution of Graded Crushed Stone Pavement Material*. Advances in Transportation Geotechnics III **143**, 854-861.

Liu X.S., Ning J.G., Tan Y.L., Gu Q.H., 2016. *Damage Constitutive Model Based on Energy Dissipation for Intact Rock Subjected to Cyclic Loading*. International Journal of Rock Mechanics and Mining Sciences **85**, 27-32.

Ma Z.G., Guo G.L., Chen R.H., Mao X.B. 2005. *An Experimental Study on the Compaction of Water-saturated Over-broken Rock*. Chinese Journal of Rock Mechanics and Engineering **24** (7), 1139-1144.

Meng Q.B., Zhang M.W., Han L.J., Pu H., Chen Y.L., 2018. *Acoustic Emission Characteristics of Red Sandstone Specimens Under Uniaxial Cyclic Loading and Unloading Compression*. Rock Mechanics and Rock Engineering **51** (4), 969-988.

Peng R.D., Ju Y., Gao F., Xie H.P., Wang P., 2014. *Energy Analysis on Damage of Coal Under Cyclical Triaxial Loading and Unloading Conditions*. Journal of China Coal Society **39** (2), 245-252.

Singh Tarun., Jain Ashwani., Rao Seshagiri, 2016. *Rock Failure Pattern under Uniaxial, Triaxial Compression and Brazilian Loading Conditions*. Geotechnical Applications **13**, 241-249.

Wang J.J., Yang Y., Zhang H.P. 2014. *Effects of Particle Size Distribution on Compaction Behavior and Particle Crushing of A Mudstone Particle Mixture*. Geotechnical and Geological Engineering **32** (4), 1159-1164.

Wang J.J., Zhang H.P., Liu M.W., Deng D.P. 2014. *Compaction Behaviour and Particle Crushing of A Crushed Sandstone Particle Mixture*. European Journal of Environmental and Civil Engineering **18** (5), 567-583.

Xiong D.G., Zhao Z.M., Su C.D., Wang G.Y., 2011. *Experimental Study of Effect of Water-saturated State on Mechanical Properties of Rock in Coal Measure Strata*. Chinese Journal of Rock Mechanics and Engineering **30** (5), 998-1006.

Xia D., Yang T.H., Wang P.T., Zhang P.H., Zhao Y.C., 2014. *Experimental Study of Acoustic Emission Characteristics of Dry and Saturated Rocks During Cyclic Loading and Unloading Process*. Journal of China Coal Society **39** (7), 1243-1247.

Xiao J.Q., Ding D.X., Jiang F.L., Xu G., 2010. *Fatigue Damage Variable and Evolution of Rock Subjected to Cyclic Loading*. International Journal of Rock Mechanics & Mining Sciences **47** (3), 461-468.

Yu B.Y., Chen Z.Q., Wu J.Y., Li Q., Ding Q.L., 2016. *Experimental Study of Compaction and Fractal Properties of Grain Size Distribution of Saturated Crushed Mudstone with Different Gradations*. Rock & Soil Mechanics **37** (7), 1887-1894.

Yu B.Y., Chen Z.Q., Dai Y.W., Xu M.M., Wei J.J., 2018. *Particle Size Distribution and Energy Dissipation of Saturated Crushed Sandstone Under Compaction*. Journal of Mining & Safety Engineering **35** (1), 197-204.

Zhu X.J., Li Y.Y., Wang C.X., Sun X.Z., Liu Z.X., 2019. *Deformation Failure Characteristics and Loading Rate Effect of Sandstone Under Uniaxial Cyclic Loading and Unloading*. Geotechnical and Geological Engineering **37** (3), 1147-1154.

Zha J.F., Guo G.L., Wang Q., Ma Z.G., 2009. *Study of In-situ Sieving Experiment and Gradation Optimization of Gangue*. Procedia Earth and Planetary Science **1** (1), 754-759.

Zhou N., Han X.L., Zhang J.X., Li M., 2016. *Compressive Deformation and Energy Dissipation of Crushed Coal Gangue*. Powder Technology **297**, 220-228.